Acta Materialia 133 (2017) 55–67

Contents lists available at ScienceDirect

Acta Materialia

journal homepage: www.elsevier.com/locate/actamat

Full length article

Enhancement of high-temperature strength of Ni-based films by addition of nano-multilayers and incorporation of W

Chao Zhang [a, b], Kai Feng [a, b, c, *], Zhuguo Li [a, b, **], Fenggui Lu [a, b], Jian Huang [a, b], Yixiong Wu [a, b], Paul K. Chu [c]

[a] Shanghai Key Laboratory of Materials Laser Processing and Modification, School of Materials Science and Engineering, Shanghai Jiao Tong University, Shanghai, 200240, China
[b] Collaborative Innovation Center for Advanced Ship and Deep-Sea Exploration, Shanghai, 200240, China
[c] Department of Physics and Materials Science, City University of Hong Kong, Tat Chee Avenue, Kowloon, Hong Kong, China

ARTICLE INFO

Article history:
Received 5 February 2017
Received in revised form
17 May 2017
Accepted 19 May 2017
Available online 21 May 2017

Keywords:
Multilayer
Ni-based film
Thermal stability
Phase separation
Hardness

ABSTRACT

Nanocrystalline Ni thin film exhibits poor thermo-mechanical properties due to its unstable microstructure at elevated temperature. Here, the paper endows a new approach to solve above issue *via* addition of nano-multilayers and incorporation of W for nanocrystalline Ni-based films, to provide novel Ni/Ni_3Al-W nano-composite multilayered structure with high hardness and good thermal stability. The thermal evolution of microstructure and mechanical properties was investigated to reveal nanocrystalline stability and strengthening mechanisms for co-sputtered Ni/Ni_3Al-W multilayers with varied W concentrations and annealing temperature. The lamellar structure and nonequilibrium phases are well maintained in 600 °C annealed multilayers, while nano-grains are further refined with increasing W addition. Annealing at 800 °C results in the appearance of elemental redistribution and phase separation in multilayers, leading to the layered structure dissolved and globular W-related particles precipitated. Annealing hardening is founded in most of annealed Ni/Ni_3Al-W multilayers. Based upon microstructure observation, grain boundary relaxation and W-related phase precipitation are mainly responsible for the hardness enhancement of multilayers at 600 °C and 800 °C, respectively. Notably, the best hardness is achieved at the value of 15.6 GPa for 800 °C annealed 12.5 at% W doped Ni/Ni_3Al-W multilayer, which shows the residual layer interfaces with larger precipitations in microstructure. This hardness increment for annealed Ni-based multilayers can be attributed that the high degree of strengthening is provided by a combination of hardening precipitation and survived lamellar structure *via* the Orowan mechanisms, offering a feasible insight to develop nano-metallic coatings for further increasing thermo-mechanical properties.

1. Introduction

Microelectromechanical systems (MEMS) can be used in harsh environments at high temperature. Advanced metallic systems are especially attractive to MEMS-scale sensing and power applications due to the electrical and thermal conductivity, strength, ductility and toughness [1–3]. Although nickel films have been widely studied in load-bearing MEMS application, they suffer from microstructure instability and property degradation due to rapid growth of nanocrystalline grains at a high temperature thus hampering their use in power generation devices, thermal actuators, and so on [4–6]. By adding alloying elements and new phases, it is possible to enhance the thermal stability and thermo-mechanical properties of Ni-based films [7–10]. In particular, alloying with W can enhance the hardness and thermal stability of nano-grains [11,12]. For example, A.J. Detor et al. [13,14] investigated the solute distribution in nanocrystalline Ni-W and found that the high solubility of W in Ni facilitated by solid solution strengthening. Moreover, the volume fraction of some W-related precipitation phases in Ni films can be increased at larger W

* Corresponding author. Shanghai Key Laboratory of Materials Laser Processing and Modification, School of Materials Science and Engineering, Shanghai Jiao Tong University, Shanghai, 200240, China.
** Corresponding author. Shanghai Key Laboratory of Materials Laser Processing and Modification, School of Materials Science and Engineering, Shanghai Jiao Tong University, Shanghai, 200240, China.
E-mail addresses: fengkai@sjtu.edu.cn (K. Feng), lizg@sjtu.edu.cn (Z. Li).

http://dx.doi.org/10.1016/j.actamat.2017.05.037
1359-6454/

Table 1
Important magnetron sputtering parameters and the elements composition of multilayers.

Samples	W target power (W)	Elements compositions (at %)	
		Ni-W layers	Ni_3Al-W layers
Ni/Ni_3Al	0	Ni 100	Ni 75.7; Al 24.3
Ni/Ni_3Al-W (4.5 at%)	145	Ni 95.5; W 4.5	Ni 71.2; Al 24.3; W4.5
Ni/Ni_3Al-W (12.5 at%)	431	Ni 87.5; W 12.5	Ni 63.9; Al 23.6; W 12.5
Ni/Ni_3Al-W (20.6 at%)	742	Ni 79.4; W 20.6	Ni 56.5; Al 22.9; W 20.6

concentrations producing excellent hardness by means of anneal strengthening. C. Borgia [15] achieved very high hardness (i.e. 16 GPa) by introducing 75 at% W to Ni thin films to form harder phases such as α-W and Ni_4W by annealing at 800 °C. However, some of intrinsic physical properties are compromised if the amount of W is excessive [16]. In this respect, the combined adoption of a multilayered structure may produce better excellent thermo-mechanical properties without the presence of a large concentration of W.

Nanoscale multilayers have produce the desirable strength and ductility on metals. Specifically, the strength and ductility of metallic multilayers are attributed to the modulation periods and choice of the constituent layers [17,18]. Generally, the hardness of multilayered thin films with equal individual layer thickness (h) improves with decreasing h. The dominant strengthening mechanism of these multilayers has been systematically studied. The Hall-Petch (H-P) relation, confined layer slip (CLS) model, and interface crossing model have been suggested to explain the strength of multilayered thin films with h ranging from micrometer to a few nanometers [19,20]. Nanoscale Ni/Ni_3Al multilayers have a high density of layer interfaces which act as barriers to grain growth. The dislocation movement is also confined at length scales from a few tens of nanometers down to a few nanometers leading to strength enhancement [21–24]. The thermal stability and strength of Ni/Ni_3Al have been studied at elevated temperature. In our previous study, Ni/Ni_3Al multilayer with h = 40 nm had high hardness (5.27 GPa) and thermal stability at 700 °C [25]. Hence, in order to obtain the optimal thermo-mechanical properties for the multilayered geometry, 40 nm is adopted as h for the W-doped nano-multilayers in this study. Addition of different W concentrations of h = 40 nm to the Ni/Ni_3Al multilayers accounts for enhancement of mechanical properties of the Ni-based films due to the refined grain size and precipitation of W-related phases in the nanoscale multilayers.

The objective of the present study is to understand the effects of W concentrations on the evolution of the microstructural and mechanical properties of W-doped Ni/Ni_3Al multilayer systems at elevated temperature. Thermal treatment is performed to simulate thermal cycles and modulate the microstructural evolution between the as-deposited and post-annealed states. The microstructure and properties of the multilayers are investigated by cross-sectional transmission electron microscopy (XTEM), X-ray diffraction (XRD), and nanoindentation. The mechanism of anneal hardening is investigated to provide the strategy to design nano-metallic coatings with excellent high-temperature strength.

2. Experimental details

W doped Ni/Ni_3Al multilayered films (hereafter referred as Ni/Ni_3Al-W multilayers) were deposited on a Si (100) wafer with a 300 nm thick SiO_2 diffusion barrier layer by direct-current (DC) magnetron sputtering. The substrate was ultrasonically cleaned and dried. Before deposition, the vacuum chamber was evacuated to a base pressure of 5×10^{-6} Torr and sputter etching was carried out in an Ar environment at a bias voltage of −300 V for 30 min to remove surface contaminants from the substrate. Deposition of the Ni/Ni_3Al-W multilayers was conducted at a pressure of 2×10^{-3} Torr (75 sccm Ar flow rate) using a pure Ni (99.99%) target, Al (99.99%) target, and W (99.99%) target. The modulated Ni_3Al-W layers were deposited through co-sputtered Ni, Al and W targets. The power of Ni and Al targets was set at 1020 W and 430 W, respectively. The corresponding Ni-W layers were derived of Ni and W co-sputtering with Ni target power at 1020 W. Simultaneously, W target power varies from 120 W to 750 W as tuning of W concentrations. Thus, the modulated layered structure was prepared *via* alternation of sputtering/closing Al target. According deposition rates for different W target powers, the time of sputtering Al target was adjusted to maintain h = 40 nm. During deposition, the first layer on the substrate was Ni-W and the top layer was Ni_3Al-W on surface, and the total film thickness is about 1.3 μm. The important processing parameters and chemical composition of the films are listed in Table 1. After sputtering, the films were annealed in an encapsulated vacuum quartz tube at $< 1 \times 10^{-5}$ Torr for 2 h at 600 °C and 800 °C, respectively. In order to avoid delamination from thermal stresses, a heating/cooling rate of 5 °C/min was adopted above 300 °C while below this temperature; the samples were allowed to cool naturally to ambient temperature.

The microstructure of the Ni/Ni_3Al multilayer films was investigated by X-ray diffraction (XRD) and transmission electron microscopy (TEM). XRD was performed on the Rigaku D/max 2500 diffractometer with Cu K_α radiation (λ = 0.15406) at room temperature with an angle range of 2θ = 30–80°. The simple estimation of grain sizes, or crystallite sizes, was chosen by applying

Table 2
Information about the average grain size d calculated by Scherrer's equation, and phase compositions of Ni/Ni_3Al-W multilayers deduced from the XRD patterns.

Conditions	W concentrations (at%)	d (nm)	Identified phases
As-deposited	0	15.1	γ-Ni(Al)
	4.5	8.7	γ-Ni(Al,W)
	12.5	6.1	γ-Ni(Al,W)
	20.6	4.3	γ- Ni(Al,W) + β-W
600 °C annealed	0	21.4	γ-Ni(Al)
	4.5	13.9	γ-Ni(Al,W)
	12.5	8.9	γ- Ni(Al,W) + β-W+α-W
	20.6	7.4	γ- Ni(Al,W) + β-W+α-W + Ni_4W + NiW
800 °C annealed	0	75.3	γ-Ni(Al)
	4.5	39.5	γ-Ni(Al,W)
	12.5	26.7	γ-Ni(Al,W)+α-W + Ni_4W + NiW
	20.6	20.3	γ-Ni(Al,W)+α-W + Ni_4W + NiW

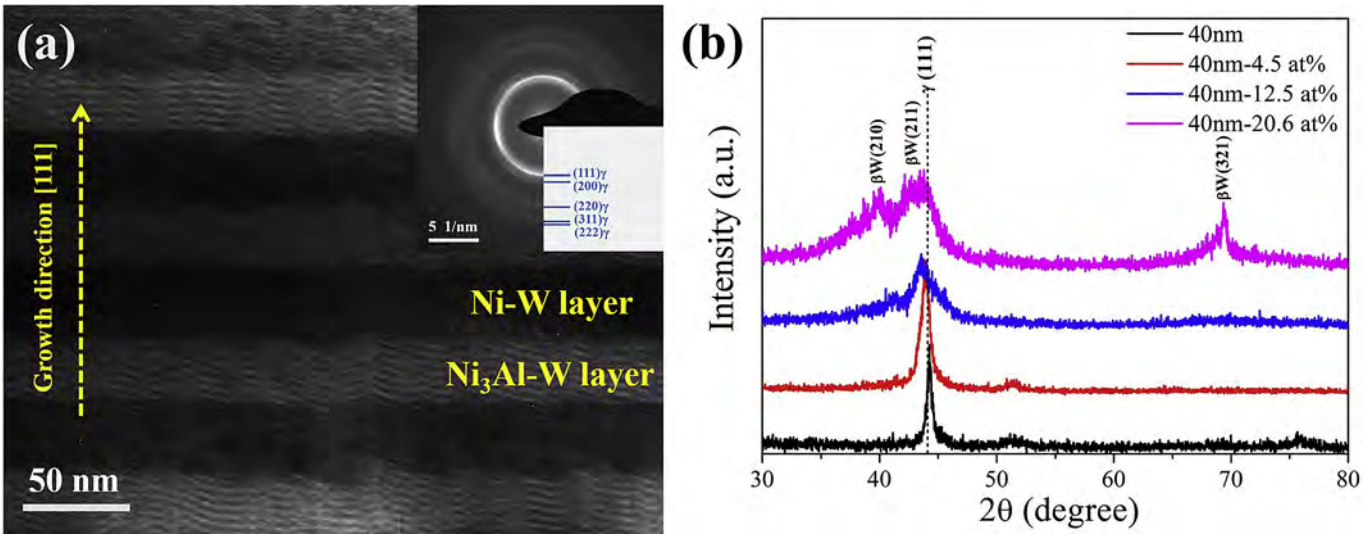

Fig. 1. The XTEM and XRD characterization of as-deposited multilayers: (a) Bright-field XTEM micrograph of representative Ni/Ni_3Al-W (12.5 at%) multilayers and corresponding selected-area electron diffraction (SAED) patterns shown in the inset; (b) XRD profiles of the as-deposited Ni/Ni_3Al-W multilayers at W concentration ranging from 0 to 20.6 at%.

Scherrer's equation [26,27] $d_{XRD} = K\lambda/\beta \cos\theta$ directly to the residual broadening β_{hkl} with $\lambda = 1.5406$ nm and shape factor $K = 0.9$. Instrumental peak broadening was accounted for by deducting 0.1° from the observed FWHM (full width half maximum) according to $\beta_{hkl} = [(\beta_{hkl})^2_{obs.} - (\beta_{hkl})^2_{instri.}]^{1/2}$ with $(\beta_{hkl})_{obs.}$ = observed FWHM, $(\beta_{hkl})_{instr.}$ = instrumental peak broadening [28,29]. The crystallite size was obtained from the highest intensity reflection at 30–80° for the respective phase and the calculated values are listed in Table 2. The peak broadening effects originating from other sources were neglected in this process [30]. Moreover, grain boundaries were contoured manually in the dark field TEM (DF-TEM) micrographs with diffraction contrast. The grain size histograms were provided by using ImageJ software as assuming spherical grains. In total, around 200 grains were measured in each of 800 °C annealed multilayers.

The cross-sectional TEM (XTEM) samples were prepared by mechanical grinding and polishing followed by thinning to an electron transparent thickness by low-energy (3.5 keV) Ar ion milling and subsequent ion polishing (Gatan PIPS, model 691). The modulation and interface of the cross-sectional multilayers were observed by TEM (FEI Tecnai G^2 F20 S-TWIN) at 200 kV. Scanning transmission electron microscopy (STEM) and energy dispersive X-ray spectroscopy (EDS) line-scan analyses were carried out to identify the elemental composition using a Fischione ultra-high resolution a high angle annular dark field (HADDF) detector with 0.23 nm special resolution in the STEM imaging mode and Oxford instruments EDS detector with a spatial resolution of ~1 nm for chemical analysis.

In order to reflect the mechanical properties varying the microstructures of Ni/Ni_3Al-W multilayers, the hardness were determined on the TI950 Tribo Indenter (Hysitron, Minneapolis, MN) equipped with a Berkovich indenter standard Berkovich tip at room temperature. To eliminate the effects of the hard substrate, the peak load was 1.5 mN by employing the load-controlled mode and the penetration depth was no more than 10% of the total coating thickness. 20 indents were performed on every sample, and the space between each indent was 100 μm to minimize the deviation of results. 95% certainty *via* the student *t*-test was calculated for the displayed error bars. Each test was set at a loading rate of 0.1 mN/s and the unloading rate of 0.05 mN/s. The holding time of 20 s at the maximum load was selected to saturate the creep effects before unloading. To improve the reliability and accuracy of the measurements, drift correction of the load-displacement curves was performed based on the mean value of the pre- and post-indentation drift calibration data collected during a holding time of 60s. The hardness of the multilayered films for each load was derived from the load depth indentation curves using the Oliver and Pharr method [31] assuming a Poisson ratio of 0.3 for both the as-deposited and annealed films.

3. Results

The microstructure of the multilayers prior to the heat treatment was characterized by XRD and TEM. The bright-field XTEM micrograph of as-deposited Ni/Ni_3Al-W (12.5 at%) multilayer are shown in Fig. 1a and the corresponding selective-area electron diffraction (SAED) patterns are depicted in the inset in Fig. 1a. The Ni-W and Ni_3Al-W layers are alternating with an equal thickness of 40 nm. After careful observation, the sublayers at size of ≤5 nm are founded within each layers. This can be attributed to the variations of target-substrate distances at 10 rpm rotation during deposition. A rotation speed of 200 rpm or higher is needed to eliminate sublayer and then obtain the uniform layers [32]. SAED indicates that the Ni-W and Ni_3Al-W layers are Ni-based fcc supersaturated solid solution (γ phase) such as Ni(W) and Ni(Al,W) phases with the (111) texture. The dual amorphous-nanocrystalline phases are observed by the broad halo of the amorphous phase and discrete rings of the γ phase. The first halo consists of two diffuse and overlapping rings of some amorphous phase [33]. The sputtering process could produce non-equilibrium structures and promote the formation of the supersaturated γ phase and amorphous phase [34]. Fig. 1b presents the XRD patterns of as-deposited Ni/Ni_3Al-W multilayers with W concentration between 0 and 20.6 at%. The dominant reflections from γ(111), (200), and (220) are observed from as-deposited Ni/Ni_3Al and Ni/Ni_3Al-W (4.5 at%) multilayers. As the W concentration goes up, the γ(111) peak becomes broader gradually indicative of a reduced grain size. At W concentration ≥12.5 at%, attenuated and broad peaks of the amorphous phases can be detected at 2θ between 36° and 46°, indicating rather low level of crystallization in the as-deposited multilayers.

Fig. 2 shows the strong effect of W concentrations on the phase transformation in the annealed Ni/Ni_3Al-W multilayers. Both

600 °C annealed Ni/Ni_3Al and Ni/Ni_3Al-W (4.5 at%) multilayers show the γ phases with fully crystallized structures. However, for 600 °C annealed Ni/Ni_3Al-W (12.5 at%) and Ni/Ni_3Al-W (20.6 at%) multilayers, the diffraction peaks of the W-related phases such as β-W, α-W, Ni_4W, and NiW emerge as the beginning of phase separation in the supersaturated γ phase. Meanwhile, the γ(111) peaks shift to smaller Bragg diffraction angles and broader width at 2θ ranging from 43° to 46°. The γ phase with increasing lattice parameters and smaller grain size is observed with W addition as shown in Fig. 2b. The (211) peak of the Ni_4W intermetallic phase overlaps the γ (111) peak in 600 °C annealed Ni/Ni_3Al-W (20.6 at%) multilayer.

After annealing at 800 °C and as shown in Fig. 2c and d, all the films are completely crystallized and peak narrowing is observed. Similar to 600 °C annealed multilayers, only the γ phase is present and there is a highly textured (111) plane without precipitation at W concentration ≤ 4.5 at%. At the increasing W concentrations, the grain orientations are more random with respect to both the Ni-rich γ and W-related precipitated phases. The β-W peaks are not detected due to its low thermal stability at 800 °C. It has been reported that significant amount of α-W phases are produced by phase transformation of the β-W phase after the heat treatment [15]. Thus, W addition promotes phase separation in the nanocrystalline Ni/Ni_3Al-W multilayers at elevated temperature as revealed by XRD.

More information about the role of W in the thermally driven structural changes in the Ni/Ni_3Al-W multilayers is obtained by XTEM. Fig. 3a displays representative BF-TEM images of 600 °C annealed Ni/Ni_3Al-W (4.5 at%) multilayer. The multilayered morphology is maintained as shown by the bright and dark regions in contrast revealing Ni-W and Ni_3Al-W layers with $h = 40$ nm. Close examination of the BF image reveals that the Ni-W layers have fully crystallized as coarsened grains with size of over 20 nm leading to dissolution of the sublayers in the Ni-W layers. The corresponding SAED pattern (inset in Fig. 3a) confirms that γ phase is present as in-plane (111) texture with the bright region around each diffraction ring. The [111] growth direction is vertical to the layer interfaces as indicated by the arrow. For 600 °C annealed Ni/Ni_3Al-W (12.5 at%) multilayer, Fig. 3b does not show any changes in the morphology indicating its excellent stability of the grains and layer structures. The very fine particles in dark contrast are dissipated, especially in the Ni-W layers, implying that the precipitated phases are nucleated. In contract, both broad halo and discrete rings are observed, verifying the coexistence of amorphous and nanocrystalline structures as shown in inset in Fig. 3b. Hence, alloying with W can reduce crystallization of the multilayers and

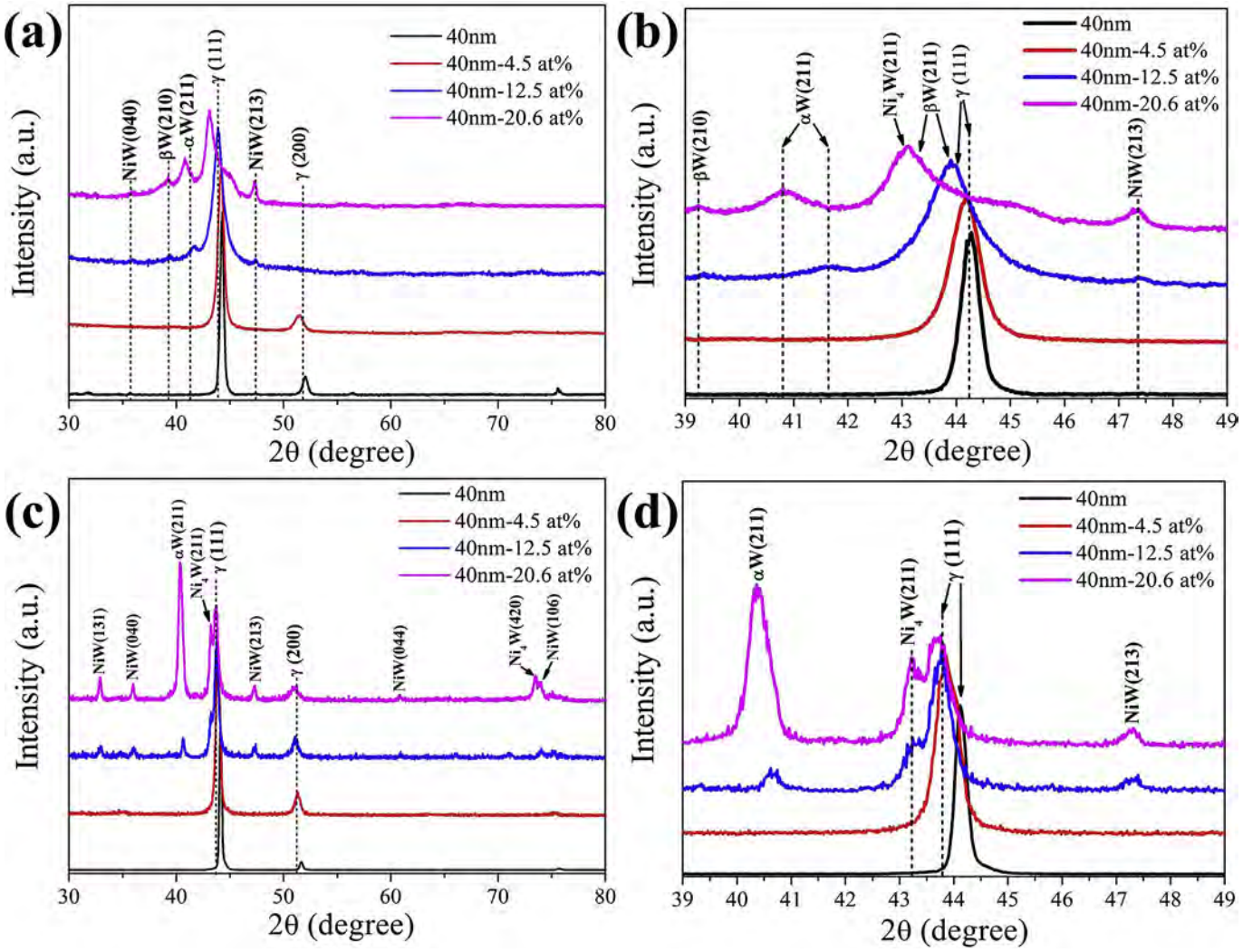

Fig. 2. XRD spectra of Ni/Ni_3Al-W multilayers with different W concentrations: (a) Annealed at 600 °C, (c) annealed at 800 °C, (b) and (d) showing the detailed feature of the profiles ranging from 39° to 49° for 600 °C and 800 °C annealed multilayers, respectively.

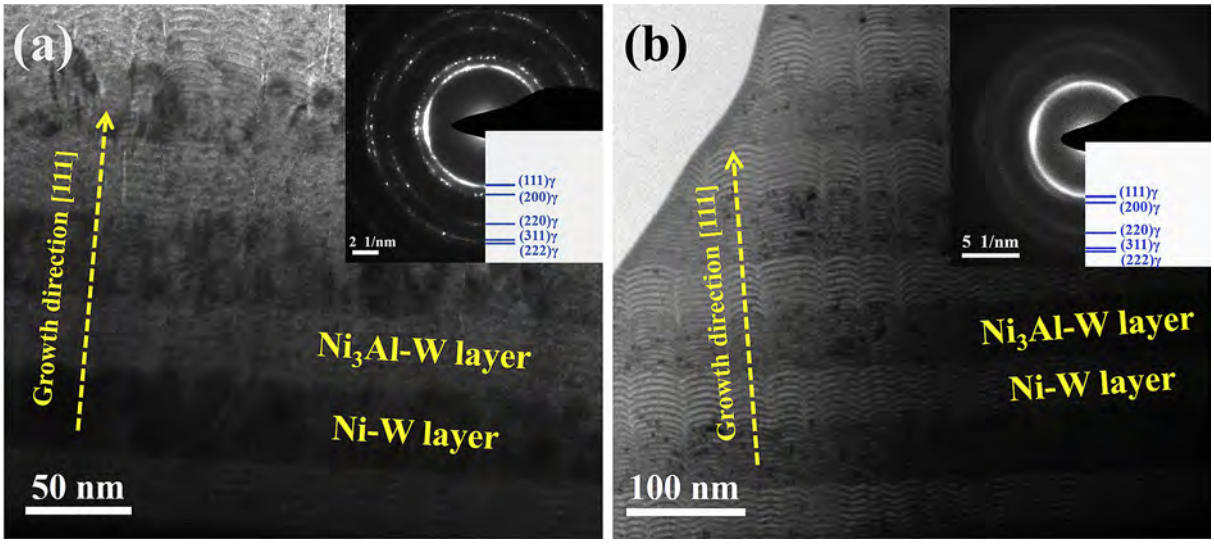

Fig. 3. Cross-sectional TEM results of the representative 600 °C annealed Ni/Ni_3Al-W multilayers: (a) Bright field image of 4.5 at% W-added multilayers and corresponding SAED patterns as shown in inset; (b) Bright field image of the 12.5 at% W-added multilayers and corresponding of SAED patterns shown in inset.

enhance the thermal stability of the metastable phases at 600 °C. As demonstrated in Fig. 4a, the lamellar structures are dissolved and the scattered particles are coarsened for 800 °C annealed Ni/Ni_3Al-W (4.5 at%) multilayer. However, a part of the layered structure survives at 800 °C (shown in Fig. 4b) indicating that addition of 12.5 at% W can produce more stable multilayers at a high temperature. Combined with the SAED patterns in the inset of Fig. 4a–c, it is confirmed that the grains are fully crystallized and coarsened because the diffraction lines sharpen eventually forming discrete spots with fewer grains. The diffraction rings of α-W and Ni_4W phases are identified from the discrete rings of both 800 °C annealed Ni/Ni_3Al-W (12.5 at%) and (20.6 at%) multilayers providing evidence of phase separation.

The dark-field (DF) TEM images of 600 °C and 800 °C annealed Ni/Ni_3Al-W multilayers in Fig. 5 provide more evidence about the evolution of the grain morphology. The bigger grains nearly 50 nm in size demonstrate abnormal growth of 600 °C annealed Ni/Ni_3Al-W (4.5 at%) multilayer. By increasing the W concentrations, the layer structures are integrated and grain growth is mostly suppressed against the in-plane of both layers and sublayers at 600 °C. After annealing at 800 °C, the very fine crystals grow into enlarging equiaxed grains without constraint of the multilayered structures. Similar to the BF image, although some grains grow across the layer interfaces, the residual layer structures are still displayed with respect to 800 °C annealed Ni/Ni_3Al-W (12.5 at%) multilayer. The actual grain size distributions extracted from the DF-TEM images for 800 °C annealed Ni/Ni_3Al-W multilayers are given in Fig. 6. A significant change in the microstructure caused by W addition is grain refinement. The 4.5 at% W multilayer have a wide grain size range of 10–90 nm and an average grain diameter of 47 nm. Addition of 12.5 at% W reduces the average grain size to 31 nm and increasing the W concentration to 20.6 at% causes the average crystalline size to shift only slightly to 25 nm, indicating that it is more difficult to further reduce the grain size by continued W addition for 800 °C annealed multilayers. In brief, the aforementioned microstructural findings clearly indicate that W alloying is an effective way to maintain the nanocrystalline structure in the films at elevated temperature. Then, the notable influence of the microstructural features on hardness responses of Ni/Ni_3Al-W multilayers will be presented in the following sections.

The ambient temperature hardness of as-deposited, 600 °C and 800 °C annealed Ni/Ni_3Al-W multilayers are shown in Fig. 7, as a function of annealing temperature. For as-sputtered multilayers, the hardness increases from 7.32 GPa to 9.05 GPa with W concentrations. In terms of Ni/Ni_3Al multilayer, the hardness decreases gradually with annealing temperature and reaches the smallest value of 4.76 GPa at 800 °C. On the contrary, the annealed Ni/Ni_3Al-W multilayers show increment of hardness. With 4.5 at% W, the hardness is improved by annealing at 600 °C to 11.0 GPa, whereas 800 °C annealing produces a drop in the hardness. In particular, the peak hardness is achieved at 15.6 GPa for 800 °C annealed Ni/Ni_3Al-W (12.5 at%) multilayer. The hardness of the Ni/Ni_3Al-W (20.6 at%) multilayers shows a similar tendency of strengthening in comparison of 12.5 at% W doped multilayers except slightly lower hardness at 800 °C.

4. Discussion

4.1. Thermal stability of multilayers with W addition

The as-deposited Ni/Ni_3Al-W multilayers have non-equilibrium phase compositions such as the supersaturated solid solution and amorphous phase. According to Scherrer's formula, the nanocrystalline sizes of as-deposited multilayers are below 10 nm with tendency to form amorphous phases. After annealing, the microstructure and phase of the W-doped multilayers vary with the composition for different temperature. The Ni-rich γ phase is present in both 600 °C and 800 °C annealed Ni/Ni_3Al-W (4.5 at%) multilayers without W-related precipitated phase. At 600 °C, crystallization is completed in the Ni-W layers but not the Ni_3Al-W layers. This leads to the formation of the distinct interface among the layers. However, the layer interfaces are not sharp and show the tendency of breaking down due to grain growth especially in the Ni-W layers, so that some of larger grains transverse across the interface. At 800 °C, the layered structure is dissolved due to spheroidization of grains and the sample is homogenized into a single γ-Ni(Al,W) phase. The instability of the multilayers at lower W concentration can be explained by Josell model based on minimization of interfacial and grain boundary energies [35]. W segregation at grain boundaries may occur to reduce the grain boundary energies [36–38]. However, during heating, insufficient W atoms are supplied to reduce the interfacial and grain boundary

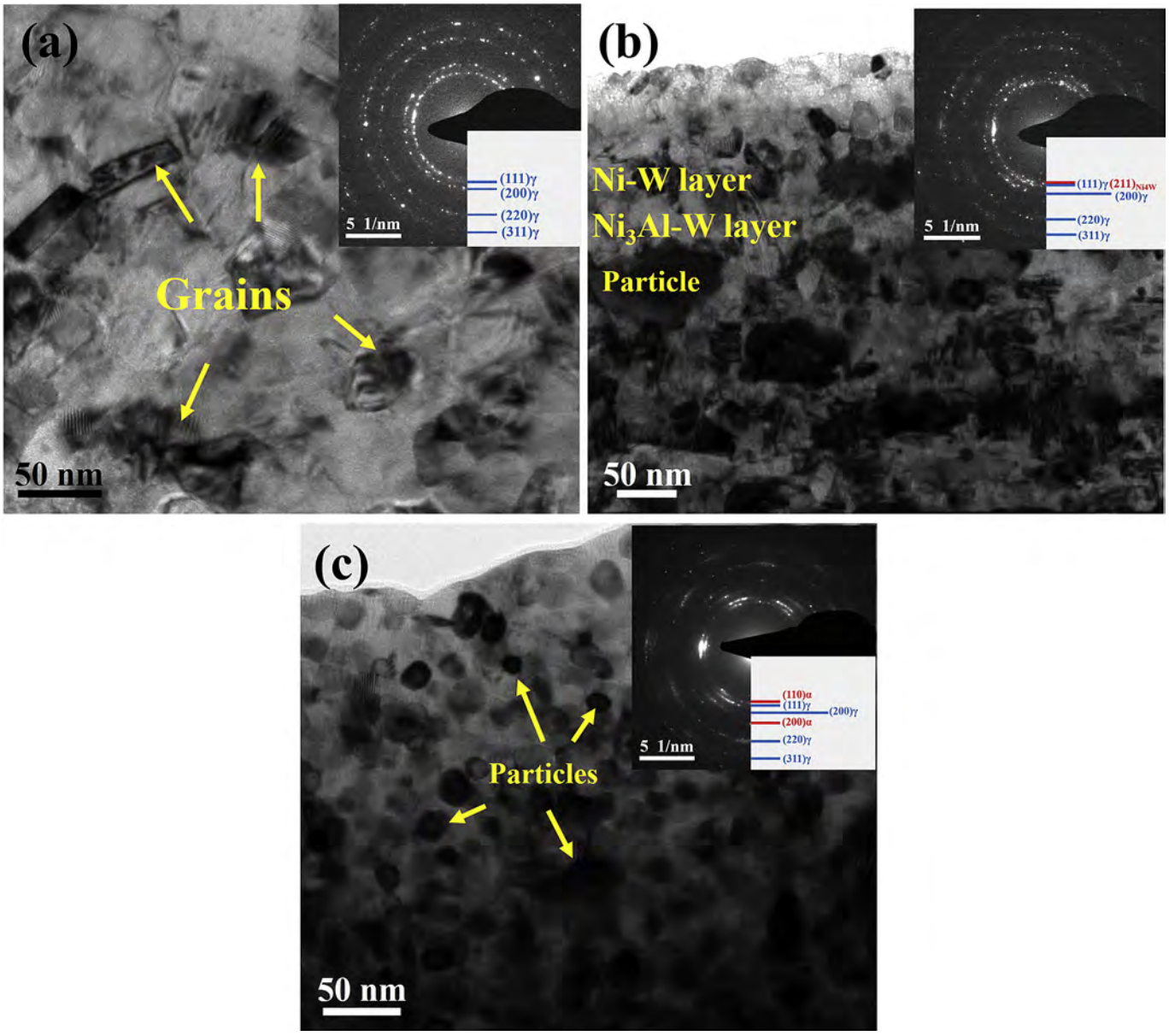

Fig. 4. XTEM results of the 800 °C annealed films, bright field images and corresponding SAED patterns in inset; (a) Ni/Ni_3Al-W (4.5 at%) multilayer (b) Ni/Ni_3Al-W (12.5 at%) multilayer and (c) Ni/Ni_3Al-W (20.6 at%) multilayer.

energies and layers with higher grain boundary energy begin to break down [39]. Consequently, the grains are coarsened and then compositions of each layers are homogenized without constraint of the layered interfaces.

At a larger W concentration ≥12.5 at%, no significant change in the grain size and lamellar morphology is observed from 600 °C annealed multilayers. The mechanisms for the high thermal stability can be ascribed to solute drag, triple junction drag, and Zener pinning. The solute drag and triple junction (TJ) drag are effective at lower annealing temperature because of enhanced grain boundary stability in the nanocrystalline materials. As shown in Fig. 8a, the intercrystalline regions (i.e., grain boundaries and triple junctions) can be identified as relatively disordered bands about 1–2 nm wide as observed by high-resolution TEM (HRTEM) of 600 °C annealed Ni_3Al-W (12.5 at%) multilayer. These intercrystalline regions such as TJs can impose drag forces for the grain boundary and have high energy densities making them the ideal places for solutes to segregate [40,41]. W segregation may occur to enhance the thermal stability by reducing the grain boundary energy but it is difficult to detect very fine grains by HRTEM here. Similar to the Cu-Ta system [42], the intercrystalline regions may also provide the pathway for W diffusion into the W-related phase, leading to a slightly higher W concentration than that in the grain interior during nanoscale W-related phase formation and growth. W-related precipitation observed by TEM also enhances stabilization by Zener pinning [43]. As shown in Fig. 8b, the HRTEM image shows that fine crystallized domains with a size of less than 5 nm are formed at 600 °C. The corresponding fast Fourier transform (FFT) of region A indicates the W-rich bcc structure consistent with the lattice spacing of β-W phase, implying that the phase separation of Ni-rich solid solution commences. In addition, the α-W phase is found from region B with a lattice space of 0.224 nm. Owing to the low thermal stability of the β-W phase, it can be treated as the transition phase that tends to transform into the α-W phases or Ni-W intermetallic phases.

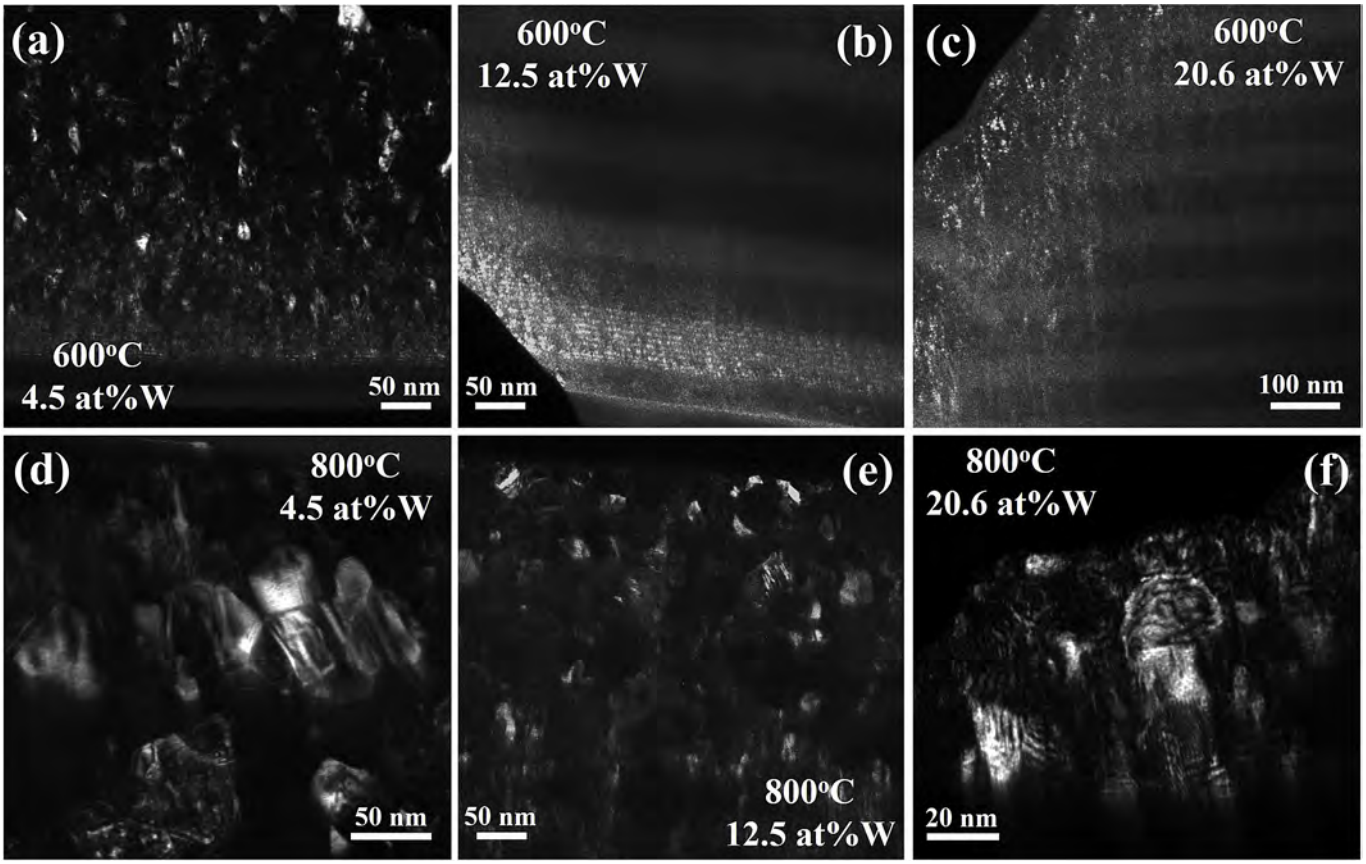

Fig. 5. Dark field TEM images of the annealed Ni/Ni_3Al-W multilayers: 600 °C annealed (a) Ni/Ni_3Al-W (4.5 at%) multilayer, (b) Ni/Ni_3Al-W (12.5 at%) multilayer, and (c) Ni/Ni_3Al-W (20.6 at%) multilayer; And 800 °C annealed: (d) Ni/Ni_3Al-W (4.5 at%) multilayer, (e) Ni/Ni_3Al-W (12.5 at%) multilayer, and (f) Ni/Ni_3Al-W (20.6 at%) multilayer.

Hence, grain growth is inhibited by the nanoscale particle pinning mechanism, as the grain size does not increase at 600 °C. Without obvious grain growth, the layer interfaces maintain the morphology. Furthermore, elemental diffusion always occurs near the layer interface and determines the thermal stability during annealing. It is thus essential to discuss the elemental distribution variations in the layers in a multilayered system.

For 600 °C annealed Ni/Ni_3Al-W (12.5 at%) multilayer at does not cause any significant mixing between constituent elements as shown by the STEM-HAADF images in Fig. 9a. The line scan profile clearly indicates that Al is mainly in the Ni_3Al-W layers, while the small amount of Al in the Ni-W layers decreases with distance from the layer surface. As a result, the Ni-W layers exhibit a slight increment of h due to small Al diffusion in the adjacent Ni_3Al-W layers. Tiny fluctuations in Ni and W are observed due to the elemental variation in the small ranges in the sublayers. These results corroborate the high thermal stability of both the sublayers and layer interfaces. With increasing annealed temperature to 800 °C, redistribution of elements is detected in 800 °C annealed Ni/Ni_3Al-W (12.5 at%) multilayer as shown in Fig. 9b. Al shows the strong tendency to homogenize and the lamellar structure is not completely damaged by chemical intermixing. For some of larger precipitates in the Ni-W layer, the interfacial layer is interrupted and the particles grow into the adjacent Ni_3Al-W layers. As shown

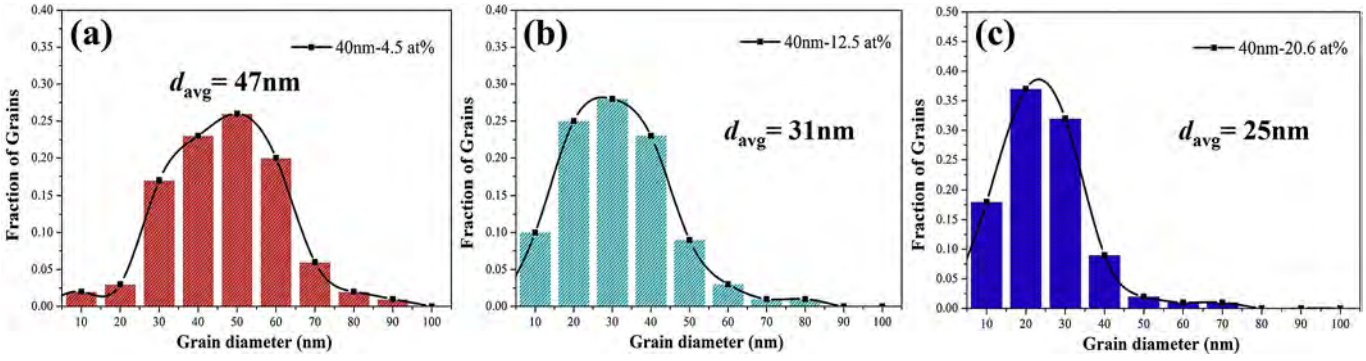

Fig. 6. Grain size distributions extracted from DF-TEM images for 800 °C annealed (a) Ni/Ni_3Al-W (4.5 at%) multilayer, (b) Ni/Ni_3Al-W (12.5 at%) multilayer, and (c) Ni/Ni_3Al-W (20.6 at%) multilayer.

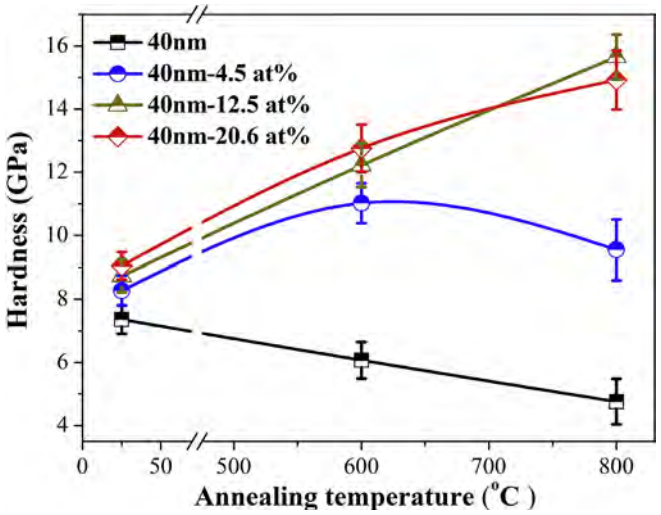

Fig. 7. Hardness measured by nanoindentation as a function of annealing temperature of the Ni/Ni_3Al-W multilayers with 0, 4.5 at%, 12.5 at% and 20.6 at% W.

in Fig. 9c, the W atoms participate in the growth of the precipitates in the Ni-W layers thereby reducing the W concentration in the Ni_3Al-W layers. Hence, W-related particles preferentially agglomerate in the Ni-W layers showing the tendency to pinch off the adjacent Ni-W layers. To better discuss the stability of the lamellar structure in relation to the size, distribution, and phases of W-related particles for multilayer at W concentrations ≥12.5 at%, HRTEM is conducted to reveal details about the precipitate. As shown in Fig. 10a, the size of the particles is about 30 nm and the adjacent layer interfaces are dissolved. Fast Fourier transform (FFT) of the square box reveals that the phase is Ni_4W with the tetragonal structure in the I4/m (87) space group. Based on STEM-HADDF and HRTEM, a fraction of the W atoms for particle growth are derived from decomposition of the γ phase especially in the Ni-W layers, while other W atoms in the adjacent Ni_3Al-W layers migrating across the interrupted layer interface. These W atoms can be combined with Ni atoms to form the dispersed Ni_4W nanoparticles. The larger particles are generated from coalescence of finer particles occupying different layers without layer interface constraint. This lowers the density of precipitation along with growth of larger Ni_4W particles as shown in Fig. 4b. On the other hand, the Al concentration decreases in the Ni_3Al-W layers due to diffusion, leading to the formation of less Ni(Al) solution. Hence, sufficient Ni atoms can be obtained to produce Ni-W compounds rather than the α-W phase. The Ni_4W phase is generated preferentially as a consequence of the larger ratio of Ni/W in the relative W-rich regions such as grain boundaries [36–38] and Ni-W layers during annealing. The grain boundary can be pinned by the precipitated Ni_4W particles hereby "curing" the momentary microstructure and preventing further grain coarsening to pinch off the layers. Hence, some of layer interfaces can be reserved due to slow grain coarsening and low density of Ni_4W precipitation in 800 °C annealed Ni/Ni_3Al-W (12.5 at%) multilayer.

By increasing the W concentration to 20.6 at%, the layer structures are obscure with high density of precipitated particles. The HRTEM image (Fig. 10b) shows that spherical W-rich precipitates are present and the annealing twins are observed as {111} reflections twins. As the films are annealed, surface/interface energy reduction is the dominant driving force for grain growth, leading to the formation of annealing twins. A prevalent theory on the formation of annealing twins is that they arise from growth accidents during the migration of grain boundaries [44–46]. When more W is added to the Ni-rich solution, stacking errors in the lattice lead to the formation of twin boundaries when energetically favorable conditions arise. The frequency of these growth errors is thought to be linked to the migration velocity of the boundary and therefore, at larger migration rates, the density of twin boundaries should increase. As the higher concentration W acts to reduce grain boundary mobility, this can explain the suppression of annealing twin formation thus limiting the microstructure to growth of already favorable oriented grains instead of twin nucleation to reduce the system energy. A similar mechanism of reduction in twin density has been observed by Mahajan et al. [47]. Consequently, the density of annealing twins is maintained at the low

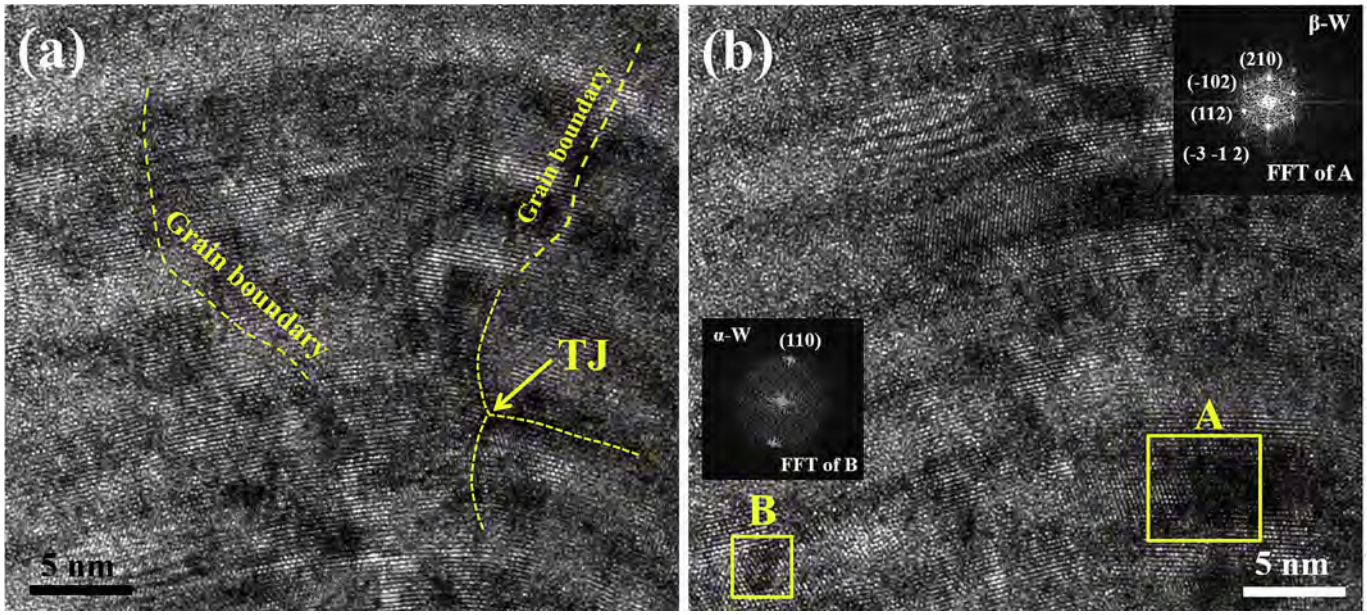

Fig. 8. HRTEM images of the representative 600 °C annealed Ni/Ni_3Al-W (12.5 at%) multilayer: (a) the intercrystalline regions (i.e., grain boundaries and triple junctions). (b) The fine crystallized domains, and corresponding FFT results are shown in insets.

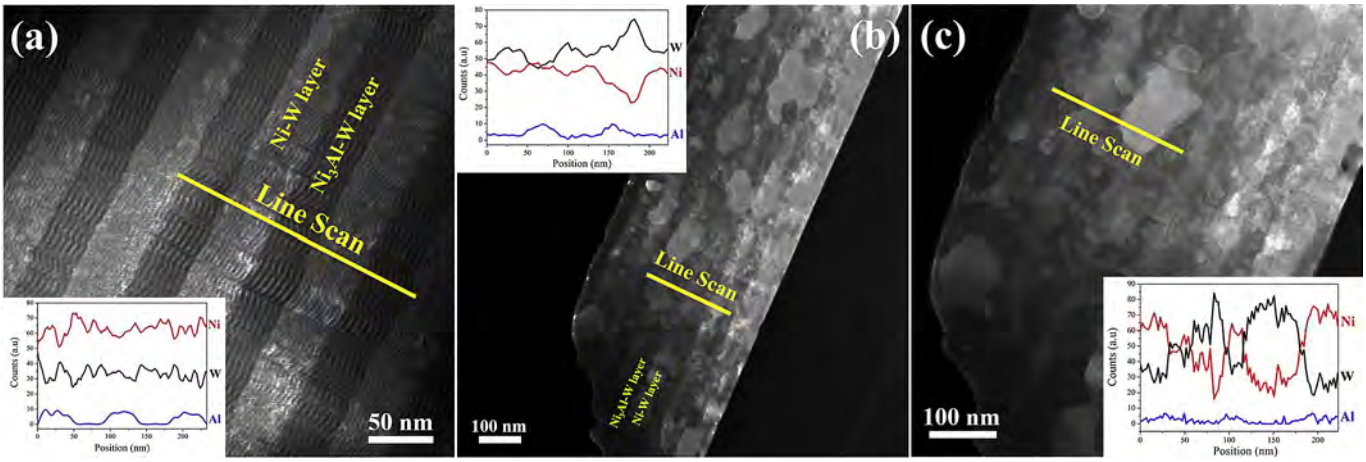

Fig. 9. The representative cross-sectional STEM-HADDF micrographs and corresponding elemental line scans in the insets. (a) 600 °C annealed Ni/Ni_3Al-W (12.5 at%) multilayer, (b) the image at low magnification of 800 °C annealed Ni/Ni_3Al-W (12.5 at%) multilayer showing the residual layer structure and precipitated particles, and (c) corresponding image at high magnification used to focus on the enlarged particles in Ni-W layers.

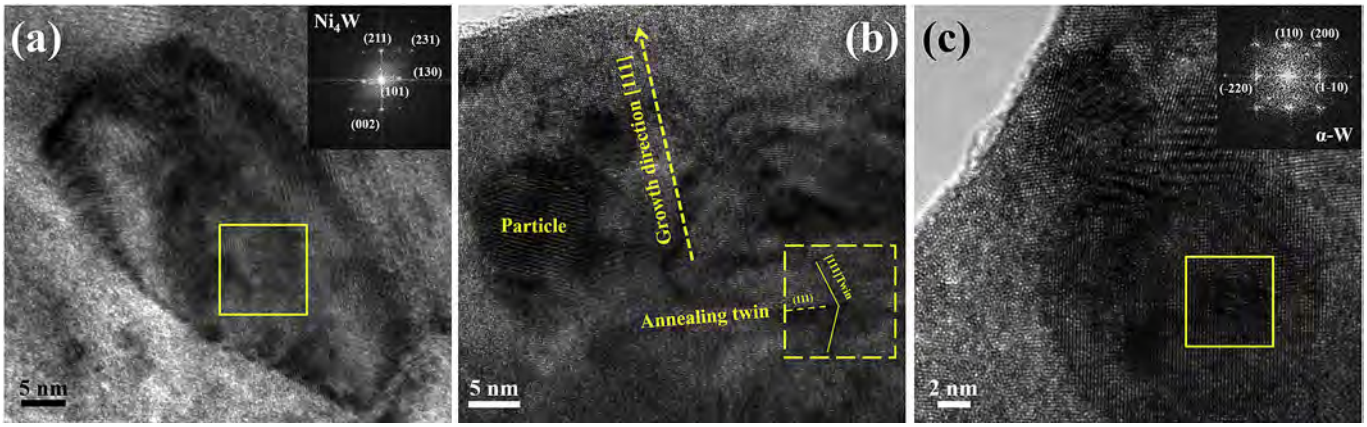

Fig. 10. HRTEM images of 800 °C annealed films: (a) the enlarged precipitated particles in Ni/Ni_3Al-W (12.5 at%) multilayer and corresponding FFT results are shown in insets. (b) The regions presented spherical particles and the annealing twins of Ni/Ni_3Al-W (20.6 at%) multilayer, and the image of spherical particles at high magnification as shown in (c).

level due to the mechanisms discussed above. However, the spheroidal precipitates are observed in common and the α-W phase is identified by FFT of the square region within the particles in Fig. 10c. Initially, the α-W phases are derived from the transformation of β-W phases and tend to coarsen with coagulation of small particles. With the decomposition of Ni-based solid solution, the excess W atoms migrate into the α-W precipitates for coarsening to reduce the surface/interface energies. The globular precipitates grow with annealing and are distributed across the whole multilayer homogeneously. The layer interfaces are pinched off easily at high density of α-W precipitates, even though the size of most particles is less than *h*. Finally, without the layer interfaces constraint, the growth of α-W phase shows the spherical shape to minimize the interface energy.

4.2. Strengthening mechanism for anneal hardening

The rule-of-mixture (ROM) is often used to estimate the hardness of nanocomposites [48,49]:

$$H_{ROM} = V_{Ni-W}H_{Ni-W} + V_{Ni_3Al-W}H_{Ni_3Al-W} \quad (1)$$

where *V* is the volume fraction with $V_{Ni-W}/V_{Ni_3Al-W} = 1$ and H_{ROM} is the hardness of the nanocomposites. By using the hardness of as-deposited monolithic Ni-W (11–13 at%) film and Ni_3Al-W (12.5 at%) film of 7–9 GPa [50] and 8.5 GPa [51], respectively, the hardness estimated by the ROM matches reasonably well the experimental value (8.7 GPa) for as-deposited Ni/Ni_3Al-W (12.5 at%) multilayer. For multilayered systems, the maximum hardness often presents higher than ROM estimations, suggesting the interface strengthening effect [52,53]. The shear modulus of two kinds of materials with larger discrepancy leads to a significant Koehler stress, which enhances the hardness of multilayers [54–56]. However, for as-deposited Ni-W and Ni_3Al-W constituents, no pronounced increase in hardness is observed for the as-deposited Ni/Ni_3Al-W multilayers. The low crystallinity with amorphous constitution is present in Ni-W and Ni_3Al-W layers, leading hardly emit dislocations from GBs with pinning pre-existing dislocations. The mechanical properties of Ni-W and Ni_3Al-W layers are also similar to each other due to their identical γ phases with same lattice. Moreover, there is no voids and delamination at the interfaces. The as-deposited Ni/Ni_3Al-W multilayers can be regarded as a kind of composite as co-deformation of two layers. Thus their hardness can be predicted by the ROM as proposed by the relevant references [48,57]. On the other hands, the hardness is increasing with W additions in comparison of as-deposited Ni/Ni_3Al multilayer. The grain refinement as Hall-Petch model accounts for this hardness enhancement more than solid solution strengthening of W element

according to the strength mechanism of Ni-W alloys reported by Schuh [58].

For annealed Ni/Ni_3Al-W multilayers, the hardness increases after annealing as consistent with that observed from the Ni-W films [15,51,59] despite some grain growth. The qualitative strengthening mechanisms are proposed by combining the effects of W concentration and annealing temperature. At a lower annealing temperature, the excess point defects and dislocations trapped in the grain boundaries are annihilated as grain boundary relaxation [60,61]. When the grain size is below 100 nm, the grain boundaries occupy a significant volume fraction of the materials. The corresponding grain boundary mediated processes evolve into plastic deformation such as grain boundary sliding. These deformation mechanisms tend to soften the materials. However, these softening effects are significantly suppressed at 600 °C. During annealing, the number of grain boundary atoms decreases and the grain boundaries relax into a more equilibrated and ordered state to provide a higher barrier for dislocation emission or grain boundary sliding thus forcing the materials to deform by dislocation gliding. Grain boundary relaxation can also occur without variation in the grain size or texture thus increasing the hardness significantly preceding obvious grain growth [62]. XRD and TEM show no noticeable microstructure change such as layer interface and grain size. Hence, a part of increment in hardness from the as-deposited state to 600 °C in the Ni/Ni_3Al-W samples can be attributed to grain boundary relaxation. Moreover, strengthening can arise from the incoherent layer interface as the barrier of dislocation movement. As shown in Fig. 11, the discrepancy of crystallization between the two layers is observed from 600 °C annealed Ni/Ni_3Al-W (4.5 at%) multilayer. The hardness after 600 °C annealing is higher than that of the as-deposited samples indicating that the discrepancy of crystallization has a reinforcement effect for the layer interfaces. The full dislocation motions are inhibited by the incoherent layer interface and then extra stress is needed to overcome the barrier from alternating in-plane stress and shear modulus. Eventually the hardness is increased. In addition, stacking faults are observed from the Ni-W layers as shown in Fig. 11 and they enhance the strength [63]. For 600 °C annealed Ni/Ni_3Al-W multilayers with W concentration ≥12.5 at%, hardening can be caused by initial precipitation from the supersaturated γ solid solution and amorphous-like phase [15]. These tiny particles can be treated as obstacles to dislocation movement responsible for the increased hardness *via* precipitation hardening.

Softening is observed from 800 °C annealed Ni/Ni_3Al-W (4.5 at %) multilayer, although grain boundary relaxation may continue to strengthen the hardness. As shown in Fig. 12, obvious grain growth with fully intermixed and completely homogenized structure is responsible for this significant reduction. Thus, the coarsened grains and absence of Koehler stress provided by the layer interface are the reasons for the softening effect. However, the strong anneal hardening behavior is present in 800 °C annealed multilayers with W concentration ≥12.5 at%. Based on the microstructure analysis by TEM, many kinds of precipitations as W-related phases play a crucial role in strengthening. The main precipitated phases such as α-W, Ni_4W have excellent hardness ranging 10 GPa from 20 GPa in the annealed Ni-W systems [64,65]. Compared to the Ni-based γ phase in the multilayers, the W-related phases can be regarded as the strengthening phases. The Orowan mechanism states that the increment of strength comes from the work needed to make the dislocations bypass the harder precipitates, although we have not clearly observed Orowan loops around the W-related precipitates [66]. The apparent lack of dislocation loops may be explained by the high contrast in the BF-TEM observation in Fig. 4b and c thereby making it difficult to observe such loops. The augment in yield

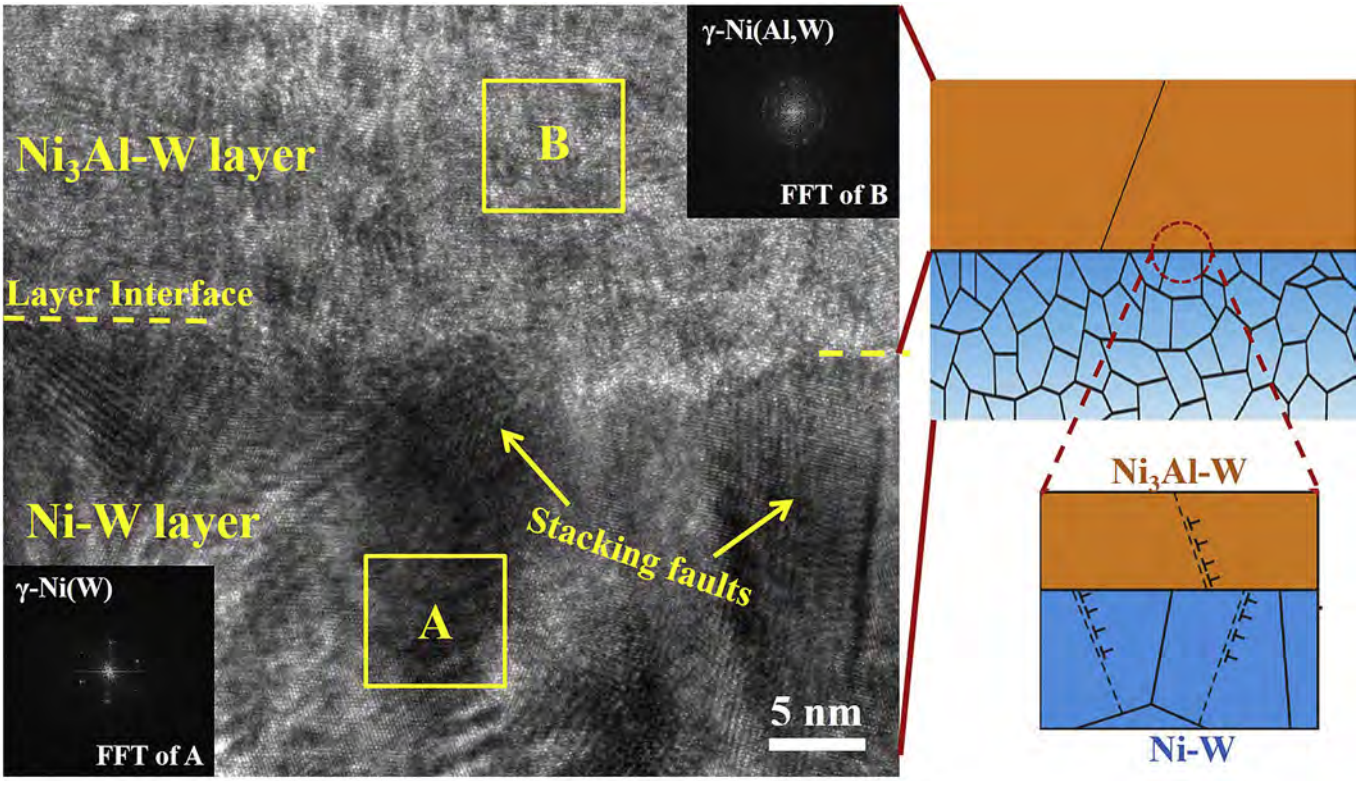

Fig. 11. HRTEM results of the regions around layer interfaces in 600 °C annealed Ni/Ni_3Al-W (4.5 at%) multilayer and schematic illustrations of the strengthening mechanisms of the incoherent interface.

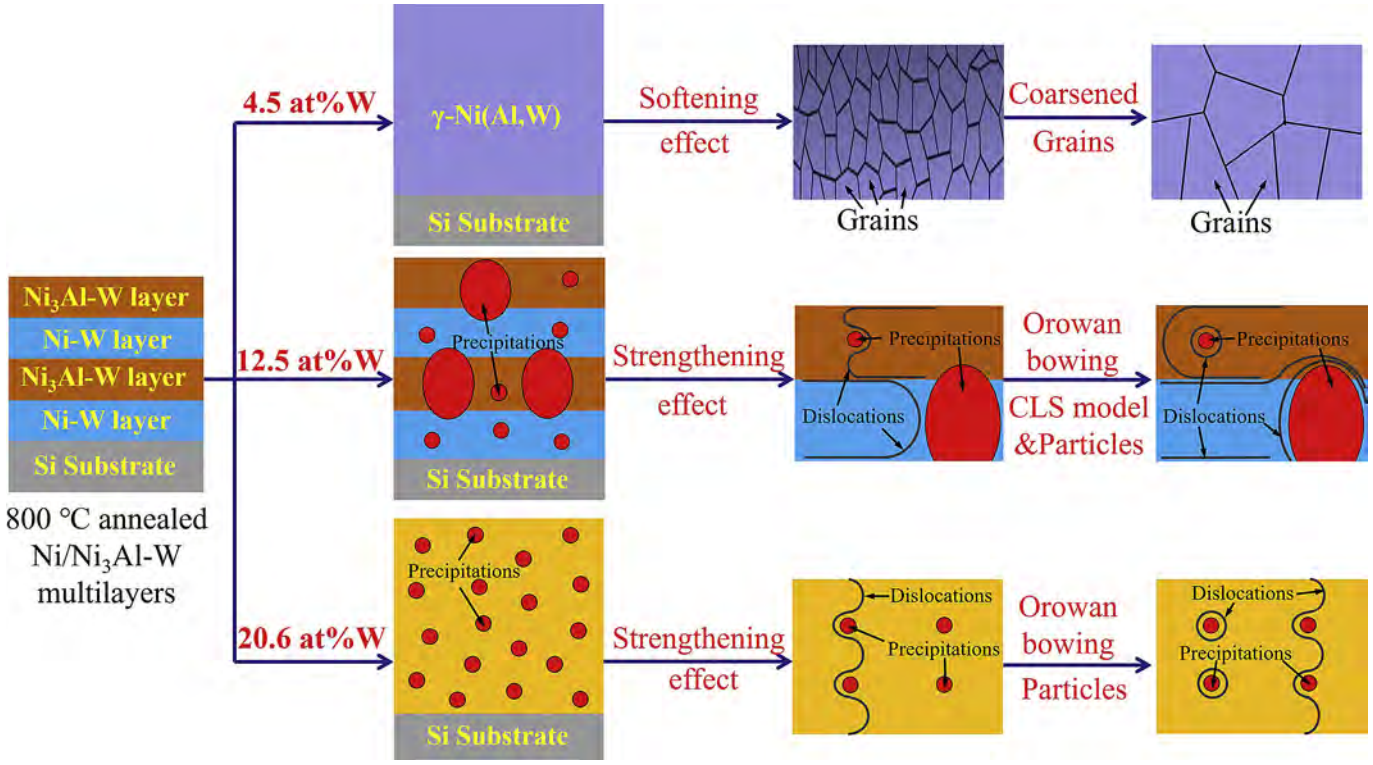

Fig. 12. Schematic illustrations of the strengthening mechanisms for anneal hardening of Ni/Ni_3Al-W multilayers at 800 °C. The red spots represent precipitations and green lines represents dislocations, respectively. (For interpretation of the references to colour in this figure legend, the reader is referred to the web version of this article.)

strength, $\Delta\sigma$, due to the Orowan mechanism in 800 °C annealed Ni/Ni_3Al-W (12.5 at%) and (20.6 at%) multilayers can be estimated by the following expression [67]:

$$\Delta\sigma = 0.4M(1-\upsilon)^{-1/2}\left(\frac{G\mathbf{b}}{\pi\lambda}\right)\cdot\ln\left(\frac{2r}{b}\right) \quad (2)$$

where λ is the inter-precipitate distance, G is the shear modulus, **b** is the Burgers vector, M is the mean orientation factor, υ is Poisson's ratio, and r is the mean precipitate radius. At 800 °C, for the Ni-based film reported in Refs. [68,69], $M \approx 3.0$, $\upsilon \approx 0.34$, G ≈ 54 GPa and $\mathbf{b} = 0.252$ nm. The values of $\lambda_1 = 19$ nm, $r_1 = 42$ nm and $\lambda_2 = 12$ nm, $r_2 = 16$ nm are derived from TEM observations of 800 °C annealed Ni/Ni_3Al-W (12.5 at%) and (20.6 at%) multilayers, respectively. The increment in strength $\Delta\sigma_1$ and $\Delta\sigma_2$ is calculated to be 1.95 GPa and 2.55 GPa, respectively. The corresponding enhancement of hardness can be estimated to be $3\Delta\sigma$ using the Tabor relation [70,71] and so approximately 6 GPa and 7.5 GPa are attributed to precipitate strengthening by the Orowan mechanism for 800 °C annealed Ni/Ni_3Al-W (12.5 at%) and (20.6 at%) multilayers, respectively.

As shown in Fig. 7, the largest hardness is observed from 800 °C annealed Ni/Ni_3Al-W (12.5 at%) multilayer. This exceptionally high hardness indicates that annealing hardening is not only determined by precipitate strengthening, but also affected by the remained layer interfaces. A confined layer slip (CLS) model has been proposed [19,72] to describe the dislocation activity and quantify the stress required to propagate a glide loop of Burgers vector confined within one layer. When h = 40 nm, dislocation pile-ups become more difficult and the movement of single dislocations is confined within the layers and the strengthening mechanism is described by the CLS model based on Orowan bowing mechanism. The critical resolved shear stressτ_{CLS} needed to initiate dislocation movement can be calculated as [73]:

$$\tau_{CLS} = \frac{G\mathbf{b}}{8\pi h}\cdot\left(\frac{4-\upsilon}{1-\upsilon}\right)\cdot\ln\left(\frac{h}{b}\right) \quad (3)$$

where h is the distance along the slip plane between adjacent interfaces equal to 56.5 nm. Using G = 54 GPa and $\mathbf{b} = 0.252$ nm, $\upsilon \approx 0.34$, for 800 °C annealed multilayers, τ_{CLS} is calculated to be 0.285 GPa. According the Tabor relation $H = 8.1\tau_{CLS}$, the hardness is 2.3 GPa. Although the layer interfaces are weaker barriers against dislocation transmission due to their degeneration at elevated temperature, they extend the density of interfaces/boundaries as barriers for dislocation slip. Thus, the calculated 8 GPa increment from the annealing harden effect is implemented by combination of precipitation and residual layer interface strengthening in 800 °C annealed Ni/Ni_3Al-W (12.5 at%) multilayer. In contrast, the contribution of annealing twins to hardening is insignificant for 800 °C annealed Ni/Ni_3Al-W (20.6 at%) multilayer due to the small density of twins.

5. Conclusion

The phase composition, microstructure, and mechanical properties of sputter-deposited and annealed Ni/Ni_3Al-W multilayers with h = 40 nm are investigated. Both the as-deposited and 600 °C annealed multilayers exhibit lamellar structure and nonequilibrium phases such as the amorphous and supersaturated solid solution phases being present with high thermal stability. The finer particles are precipitated as onset of phase separation in Ni/Ni_3Al-W multilayers at W concentration ≥12.5 at%. Therefore, W addition enhances the thermal stability of the microstructure and facilitates

phase separation. For the 800 °C annealed Ni/Ni_3Al-W (4.5 at%) multilayers, the layered structure is dissolved and the sample is homogenized. With more W addition, nano-sized Ni_4W and α-W particles are observed as dominant precipitates as a result of phase separation induced by elemental redistribution. In particular, the layer interfaces survive due to low density of precipitation in the 800 °C annealed Ni/Ni_3Al-W (12.5 at%) multilayers. Annealing strengthening depends on the temperature and W concentration. At 600 °C, grain boundary relaxation is deemed the dominant strengthening mechanism. The incoherent interface and initial precipitation as obstruction for dislocations movement are responsible for annealing hardening in the Ni/Ni_3Al-W (4.5 at%) and Ni/Ni_3Al-W (≥12.5 at%) multilayers, respectively. At 800 °C, the outstanding hardness of the Ni/Ni_3Al-W (12.5 at%) multilayers can be attributed to combination of precipitation and residual layer interface strengthening *via* the Orowan mechanisms. The Ni/Ni_3Al-W (12.5 at%) multilayer have excellent thermal stability and mechanical performance and are suitable for high-temperature MEMS applications.

Acknowledgments

Financial support from the National Nature Science Foundation of China under grant number 51201106, “Chen Guang” project Shanghai Municipal Education Commission, Shanghai Education Development Foundation (Grant Number 13CG07), “Chenxing” young scholar project of Shanghai Jiao Tong University (Grant Number 14X100010017), Hong Kong Research Grants Council (RGC) General Research Funds (GRF) No. 11301215, and City University of Hong Kong Strategic Research Grant (SRG) No. 7004644 is acknowledged.

References

[1] T.M. Lucas, E.V. Moiseeva, G. Zhang, A.M. Gobin, C.K. Harnett, Thermal properties of infrared absorbent gold nanoparticle coatings for MEMS applications, Sens. Actuat. A 198 (2013) 81–86.
[2] H. Shi, S. Fan, Y. Zhang, J. Sun, Nonlinear dynamics study based on uncertainty analysis in electro-thermal excited mems resonant sensor, Sens. Actuat. A 232 (2015) 103–114.
[3] E. Pirmoradi, H. Mirzajani, H.B. Ghavifekr, Design and simulation of a novel electro-thermally actuated lateral RF MEMS latching switch for low power applications, Microsyst. Technol. 21 (2015) 465–475.
[4] J.A. Krogstad, C. Keimel, K.J. Hemker, Emerging materials for microelectromechanical systems at elevated temperatures, J. Mater. Res. 29 (2014) 1597–1608.
[5] D.E. Burns, Y. Zhang, M. Teutsch, K. Bade, J. Aktaa, K.J. Hemker, Development of Ni-based superalloys for microelectromechanical systems, Scr. Mater. 67 (2012) 459–462.
[6] D.E. Burns, Y. Zhang, T.P. Weihs, K.J. Hemker, Properties of sputter deposited Ni-base superalloys for microelectromechanical systems, Thin Solid Films 558 (2014) 20–23.
[7] R.A. Andrievski, Review of thermal stability of nanomaterials, J. Mater. Sci. 49 (2014) 1449–1460.
[8] C.J. Tsai, K.J. Hsueh, N. Plusnin, C.C. Kuo, W.C. Lin, Growth, thermal stability and magnetism of Ni ultrathin films on O-3×3/W (111) surface, Appl. Surf. Sci. 313 (2014) 166–171.
[9] F.L. Miguel, R. Müller, S. Mathur, F. Mücklich, On the thermal stability of electrodeposited Ni-matrix-nanocomposite films reinforced with Ag-coated SnO_2 nanowires, Surf. Coat. Technol. 287 (2016) 93–102.
[10] Y. Xing, B. Dai, X. Wei, Y. Ma, M. Wang, Enhancement of high-temperature oxidation resistance and mechanical properties of Ni_3Al thin films by inserting ultrathin Cr layers, Vacuum 101 (2014) 107–112.
[11] S. Suresha, M. Haj-Taieb, K. Bade, J. Aktaa, K. Hemker, The influence of tungsten on the thermal stability and mechanical behavior of electrodeposited nickel MEMS structures, Scr. Mater. 63 (2010) 1141–1144.
[12] N. Sunwang, P. Wangyao, Y. Boonyongmaneerat, The effects of heat treatments on hardness and wear resistance in Ni-W alloy coatings, Surf. Coat. Technol. 206 (2011) 1096–1101.
[13] A.J. Detor, M.K. Miller, C.A. Schuh, Solute distribution in nanocrystalline Ni-W alloys examined through atom probe tomography, Philos. Mag. 86 (2006) 4459–4475.
[14] A.J. Detor, C.A. Schuh, Tailoring and patterning the grain size of nanocrystalline alloys, Acta Mater. 55 (2007) 371–379.
[15] C. Borgia, T. Scharowsky, A. Furrer, C. Solenthaler, R. Spolenak, A combinatorial study on the influence of elemental composition and heat treatment on the phase composition, microstructure and mechanical properties of Ni-W alloy thin films, Acta Mater. 59 (2011) 386–399.
[16] F.T.N. Vüllers, R. Spolenak, From solid solutions to fully phase separated interpenetrating networks in sputter deposited “immiscible” W-Cu thin films, Acta Mater. 99 (2015) 213–227.
[17] J.Y. Zhang, G. Liu, X. Zhang, G.J. Zhang, J. Sun, E. Ma, A maximum in ductility and fracture toughness in nanostructured Cu/Cr multilayer films, Scr. Mater. 62 (2010) 333–336.
[18] C. Gu, F. Wang, P. Huang, T.J. Lu, K.W. Xu, Altering strength and plastic deformation behavior *via* alloying and laminated structure in nanocrystalline metals, Mater. Sci. Eng. A 640 (2015) 24–32.
[19] A. Misra, J.P. Hirth, R.G. Hoagland, Length-scale-dependent deformation mechanisms in incoherent metallic multilayered composites, Acta Mater. 53 (2005) 4817–4824.
[20] J. Li, Y. Chen, S. Xue, H. Wang, X. Zhang, Comparison of size dependent strengthening mechanisms in Ag/Fe and Ag/Ni multilayers, Acta Mater. 114 (2016) 154–163.
[21] S. Tixier, P. Böni, H. Van Swygenhoven, Hardness enhancement of sputtered Ni_3Al/Ni multilayers, Thin Solid Films 342 (1999) 188–193.
[22] W.H. Xu, X.K. Meng, C.S. Yuan, A.H.W. Ngan, K.L. Wang, Z.G. Liu, The synthesis and mechanical property evaluation of Ni/Ni_3Al microlaminates, Mater. Lett. 46 (2000) 303–308.
[23] X.K. Meng, H. Shen, H. Vehoff, S. Mathur, A.H.W. Ngan, Fractography, elastic modulus, and oxidation resistance of novel metal-intermetallic Ni/Ni_3Al multilayer films, J. Mater. Res. 17 (2002) 790–796.
[24] E.A. Sperling, P.M. Anderson, J.L. Hay, Correlation of stress state and nanohardness *via* heat treatment of nickel-aluminide multilayer thin films, J. Mater. Res. 19 (2004) 3374–3381.
[25] C. Zhang, K. Feng, Z. Li, F. Lu, J. Huang, Y. Wu, Microstructure and mechanical properties of sputter deposited Ni/Ni_3Al multilayer films at elevated temperature, Appl. Surf. Sci. 378 (2016) 408–417.
[26] P. Scherrer, Bestimmung der Größe und der inneren Struktur von Kolloidteilchen mittels Röntgenstrahlen, Nachr. Ges. Wiss. Gött (1918) 98–100.
[27] U. Holzwarth, N. Gibson, The Scherrer equation versus the ‘Debye-Scherrer equation’, Nat. Nanotechnol. 6 (2011) 534.
[28] V. Mote, Y. Purushotham, B. Dole, Williamson-Hall analysis in estimation of lattice strain in nanometer-sized ZnO particles, J. Theor. Appl. Phys. 6 (2012) 1–8.
[29] B.D. Cullity, S.R. Stock, Elements of X-Ray Diffraction, third ed., Prentice Hall, 2001.
[30] M. Wilkens, Quantitative interpretation of X-ray line broadening of plastically deformed crystals, J. Appl. Crystallogr. 8 (1975) 191–192.
[31] W.C. Oliver, G.M. Pharr, An improved technique for determining hardness and elastic modulus using load and displacement sensing indentation experiments, J. Mater. Res. 7 (1992) 1564–1583.
[32] M. Callisti, F. Tichelaar, B. Mellor, T. Polcar, Effects of Cu on the microstructural and mechanical properties of sputter deposited Ni-Ti thin films, Surf. Coat. Technol. 237 (2013) 261–268.
[33] T.J. Rupert, J.C. Trenkle, C.A. Schuh, Enhanced solid solution effects on the strength of nanocrystalline alloys, Acta Mater. 59 (2011) 1619–1631.
[34] B.R. Braeckman, D. Depla, On the amorphous nature of sputtered thin film alloys, Acta Mater. 109 (2016) 323–329.
[35] D. Josell, F. Spaepen, Surfaces, interfaces, and changing shapes in multilayered films, Mrs Bull. 24 (1999) 39–43.
[36] A.J. Detor, C.A. Schuh, Grain boundary segregation, chemical ordering and stability of nanocrystalline alloys: atomistic computer simulations in the Ni-W system, Acta Mater. 55 (2007) 4221–4232.
[37] U. Welzel, J. Kümmel, E. Bischoff, S. Kurz, E.J. Mittemeijer, Nanoscale planar faulting in nanocrystalline Ni-W thin films: grain growth, segregation, and residual stress, J. Mater. Res. 26 (2011) 2558–2573.
[38] G. Csiszár, S.J.B. Kurz, E.J. Mittemeijer, Stability of nanosized alloy thin films: faulting and phase separation in metastable Ni/Cu/Ag-W films, Acta Mater. 110 (2016) 324–340.
[39] D. Srinivasan, S. Sanyal, R. Corderman, P.R. Subramanian, Thermally stable nanomultilayer films of Cu/Mo, Metall. Mater. Trans. A 37 (2006) 995–1003.
[40] P. Stender, Z. Balogh, G. Schmitz, Triple junction segregation in nanocrystalline multilayers, Phys. Rev. B 83 (2011) 121407.
[41] Y. Chen, C.A. Schuh, Contribution of triple junctions to the diffusion anomaly in nanocrystalline materials, Scr. Mater. 57 (2007) 253–256.
[42] K. Darling, A. Roberts, Y. Mishin, S. Mathaudhu, L. Kecskes, Grain size stabilization of nanocrystalline copper at high temperatures by alloying with tantalum, J. Alloy Compd. 573 (2013) 142–150.
[43] C.J. Marvel, D. Yin, P.R. Cantwell, M.P. Harmer, The influence of oxygen contamination on the thermal stability and hardness of nanocrystalline Ni-W alloys, Mater. Sci. Eng. A 664 (2016) 49–57.
[44] Q. Li, J.R. Cahoon, N.L. Richards, Effects of thermo-mechanical processing parameters on the special boundary configurations of commercially pure nickel, Mater. Sci. Eng. A 527 (2009) 263–271.
[45] J.R. Cahoon, Q. Li, N.L. Richards, Microstructural and processing factors influencing the formation of annealing twins, Mater. Sci. Eng. A 526 (2009) 56–61.
[46] J. Kacher, P. Elizaga, S.D. House, K. Hattar, M. Nowell, I.M. Robertson, Thermal stability of Ni/NiO multilayers, Mater. Sci. Eng. A 568 (2013) 49–60.
[47] S. Mahajan, C.S. Pande, M.A. Imam, B.B. Rath, Formation of annealing twins in

F.C.C. crystals, Acta Mater. 45 (1997) 2633–2638.
[48] H.S. Kim, Y. Estrin, M.B. Bush, Plastic deformation behaviour of fine-grained materials, Acta Mater. 48 (2000) 493–504.
[49] M. Callisti, T. Polcar, Combined size and texture-dependent deformation and strengthening mechanisms in Zr/Nb nano-multilayers, Acta Mater. 124 (2017) 247–260.
[50] T.J. Rupert, J.C. Trenkle, C.A. Schuh, Enhanced solid solution effects on the strength of nanocrystalline alloys, Acta Mater. 59 (2011) 1619–1631.
[51] C. Zhang, K. Feng, Z. Li, F. Lu, J. Huang, Y. Wu, P.K. Chu, Enhancement of hardness and thermal stability of W-doped Ni_3Al thin films at elevated temperature, Mater. Des. 111 (2016) 575–583.
[52] Q. Zhou, J.Y. Xie, F. Wang, P. Huang, K.W. Xu, T.J. Lu, The mechanical behavior of nanoscale metallic multilayers: a survey, Acta Mech. Sin. 31 (2015) 319–337.
[53] E.G. Fu, N. Li, A. Misra, R.G. Hoagland, H. Wang, X. Zhang, Mechanical properties of sputtered Cu/V and Al/Nb multilayer films, Mater. Sci. Eng. A 493 (2008) 283–287.
[54] J.W. Yan, G.P. Zhang, X.F. Zhu, H.S. Liu, C. Yan, Microstructures and strengthening mechanisms of Cu/Ni/W nanolayered composites, Phil. Mag. 93 (2013) 434–448.
[55] S.P. Wen, R.L. Zong, F. Zeng, Y. Gao, F. Pan, Evaluating modulus and hardness enhancement in evaporated Cu/W multilayers, Acta Mater. 55 (2007) 345–351.
[56] F.T.N. Vullers, R. Spolenak, From solid solutions to fully phase separated interpenetrating networks in sputter deposited “immiscible” W-Cu thin films, Acta Mater. 99 (2015) 213–227.
[57] J.Y. Zhang, X. Zhang, R.H. Wang, S.Y. Lei, P. Zhang, J.J. Niu, G. Liu, G.J. Zhang, J. Sun, Length-scale-dependent deformation and fracture behavior of Cu/X (X = Nb, Zr) multilayers: the constraining effects of the ductile phase on the brittle phase, Acta Mater. 59 (2011) 7368–7379.
[58] C.A. Schuh, T.G. Nieh, H. Iwasaki, The effect of solid solution W additions on the mechanical properties of nanocrystalline Ni, Acta Mater. 51 (2003) 431–443.
[59] K.H. Hou, Y.F. Chang, S.M. Chang, C.H. Chang, The heat treatment effect on the structure and mechanical properties of electrodeposited nano grain size Ni–W alloy coatings, Thin Solid Films 518 (2010) 7535–7540.
[60] A. Detor, C. Schuh, Microstructural evolution during the heat treatment of nanocrystalline alloys, J. Mater. Res. 22 (2007) 3233–3248.
[61] T.J. Rupert, J.R. Trelewicz, C.A. Schuh, Grain boundary relaxation strengthening of nanocrystalline Ni-W alloys, J. Mater. Res. 27 (2012) 1285–1294.
[62] Z. Yang, J. Wang, Coupled annealing temperature and layer thickness effect on strengthening mechanisms of Ti/Ni multilayer thin films, J. Mech. Phys. Solids 88 (2016) 72–82.
[63] D. Bufford, Z. Bi, Q.X. Jia, H. Wang, X. Zhang, Nanotwins and stacking faults in high-strength epitaxial Ag/Al multilayer films, Appl. Phys. Lett. 101 (2012) 1–6.
[64] H. Sun, Z. Song, D. Guo, F. Ma, K. Xu, Microstructure and mechanical properties of nanocrystalline tungsten thin films, J. Mater. Sci. Technol. 26 (2010) 87–92.
[65] Z. Zhong, T. Hinoki, H.C. Jung, Y.H. Park, A. Kohyama, Microstructure and mechanical properties of diffusion bonded SiC/steel joint using W/Ni interlayer, Mater. Des. 31 (2010) 1070–1076.
[66] R. Goswami, C. Pande, N. Bernstein, M. Johannes, C. Baker, G. Villalobos, A high degree of enhancement of strength of sputter deposited Al/Al_2O_3 multilayers upon post annealing, Acta Mater. 95 (2015) 378–385.
[67] C.B. Fuller, D.N. Seidman, D.C. Dunand, Mechanical properties of Al (Sc, Zr) alloys at ambient and elevated temperatures, Acta Mater. 51 (2003) 4803–4814.
[68] A. Godon, J. Creus, S. Cohendoz, E. Conforto, X. Feaugas, P. Girault, C. Savall, Effects of grain orientation on the Hall-Petch relationship in electrodeposited nickel with nanocrystalline grains, Scr. Mater. 62 (2010) 403–406.
[69] R. Dickson, J. Wachtman Jr., S. Copley, Elastic constants of single-crystal Ni_3Al from 10° to 850° C, J. Appl. Phys. 40 (1969) 2276–2279.
[70] D. Tabor, Indentation hardness: fifty years on a personal view, Philos. Mag. A 74 (1996) 1207–1212.
[71] P. Zhang, S.X. Li, Z.F. Zhang, General relationship between strength and hardness, Mater. Sci. Eng. A 529 (2011) 62–73.
[72] J.J. Niu, J.Y. Zhang, G. Liu, P. Zhang, S.Y. Lei, G.J. Zhang, J. Sun, Size-dependent deformation mechanisms and strain-rate sensitivity in nanostructured Cu/X (X = Cr, Zr) multilayer films, Acta Mater. 60 (2012) 3677–3689.
[73] A. Misra, J.P. Hirth, H. Kung, Single-dislocation-based strengthening mechanisms in nanoscale metallic multilayers, Philos. Mag. A 82 (2002) 2935–2951.